Geomechanics and Engineering, *Vol. 40, No. 3 (2025) 183-191*
https://doi.org/10.12989/gae.2025.40.3.183

Nonlinear snap-buckling of graphene platelet reinforced metal foams doubly curved shells with geometric imperfection

Gui-Lin She*, Lei-Lei Gan and Jia-Qin Xu

College of Mechanical and Vehicle Engineering, Chongqing University, Chongqing 400044, China

(*Received February 28, 2023, Revised January 12, 2025, Accepted February 3, 2025*)

Abstract. In this paper, the nonlinear bending of graphene platelet reinforced metal foams (GPLRMF) doubly curved shells is analyzed. Based on the Reddy' higher-order shear deformation theory, the nonlinear equations of motion are obtained by using Hamilton's principle, which are solved by utilizing assuming modal method and Newton-Raphson approach. In the end, the parameters are systematically studied to illustrate the effects of porosity coefficient, geometric imperfections, graphene platelets (GPLs) mass fraction, GPLs and pore distribution types on the nonlinear bending characteristics of GPLRMF doubly curved shells. It can be found that these parameters have a significant impact on this issue.

Keywords: doubly curved shell; metal foams; nonlinear bending; snap-buckling

1. Introduction

With the continuous development of industry and the continuous innovation of structural system, more and more large-span space structures are widely used in various industrial and civil buildings with their excellent space bearing capacity and novel modeling. As one of the most important structural forms, doubly curved shells are often used in large mechanical parts such as aircraft, ships, pressure vessels, etc. Moreover, as a lightweight structure, doubly curved shell structures often exhibit complex dynamics and statics response different from other structural forms under the action of external loads, which often becomes one of the main reasons for the failure of such structures. Therefore, it is greatly significant to study the dynamics and statics mechanics behavior of doubly curved shells. Tornabene *et al.* (2023) used Generalized Differential Quadrature method to analyze the linear static behavior of spherical shells under external loading. Rezaee and Yazdi (2022) predicted the influence of carbon nanotubes on the nonlinear frequency of doubly curved shells by analogy. Jing *et al.* (2022) designed the buckling laminated characteristics of doubly curved shallow shells using 2D-sampling optimization method. Tornabene *et al.* (2022) analyzed the dynamic behavior of doubly curved shells with non-uniform thickness. Vinh and Tounsi (2022) used the first-order shear deformation theory (FSDT) to analyze the free vibration response of functionally graded (FG) doubly curved shells. Aminipour and Emam (2022) used the Galerkin method to study the influence of static loads on nonlinear snap-through and bending characteristics of doubly curved shallow shells with simply supported boundary conditions. Sharma *et al.* (2021) discussed the bending response of doubly curved cylindrical and spherical composite shells to verify the feasibility of hyperbolic shear deformation theory. Liu *et al.* (2021) applied the HSDT to solve the post-buckling solutions of anisotropic doubly curved shell. With the help of HSDT, Tornabene *et al.* (2021) advanced a model to study the vibration behavior of anisotropic doubly curved shell strengthened with honeycomb cores. Meanwhile, Arefi and Amabili (2021) employed nonlocal elastic theory to illustrate the effects of electro-mechanical load on the buckling and bending response of multilayer doubly curved nano-shell. Xu *et al.* (2021) used nonlocal strain gradient theory (NSGT) to study the resonance response of FG anisotropic doubly curved nano-shell. Dai and Safarpour (2021) investigated the frequency and thermal buckling response of doubly curved nano-shell in non-uniform temperature field using NSGT. Karimiasl *et al.* (2021) explored the influence of humid and thermal environment on the post-buckling response of composite multilayer spherical shell. Huang and Qiao (2020) investigated the influence of imperfections on nonlinear stability of composite multilayer doubly curved shell under external loads. Aminipour *et al.* (2020) analyzed the propagation characteristics of waves in FG doubly curved shell using HSDT. Mirjavadi *et al.* (2020) discussed the influence of elastic foundation on the post-buckling behavior and nonlinear stability of porous doubly curved shell with geometric imperfections. Shahmohammadi *et al.* (2022) used Galerkin's method to define the effect of geometric imperfections on the nonlinear behavior of functionally graded graphene sheet reinforced composite (FG-GPLRC) doubly curved shell. Arefi *et al.* (2022) applied the HSDT to analyze the influence of elastic foundation on the bending behavior of doubly curved nano-shell. Hoang *et al.* (2021) used classical shell theory to explain the influence of elastic foundation on nonlinear vibration response of FG-GPLRC doubly curved shallow shell. Karami and Shahsavari (2020) applied the HSDT to

*Corresponding author, Professor
E-mail: sheguilin@cqu.edu.cn

ISSN: 2005-307X (Print), 2092-6219 (Online)

study the forced resonance behavior of FG-GPLRC doubly curved nano-shell. Trinh and Kim (2019) analyzed the bending behavior and free vibration response of FG porous doubly curved shell under external loads.

In practical engineering applications, many structures are affected by their own reasons or external factors, when the structural parameters change slightly, it will cause sharp changes in some modal information of the structure, that is, snap-buckling phenomenon. Because this phenomenon is difficult to be observed by the naked eye in time, it will lead to major safety accidents. Therefore, it is of inestimable engineering value to study the snap-buckling characteristics of structures. Abbasi *et al.* (2023) used the finite element analysis to study the snap-buckling behaviors of the bistable beam subject to magnetic and mechanical loads. Babaei (2022) utilized the HSDT to discuss the snap-buckling behaviors of nanocomposite cylindrical panel under uniform external loads. Atacan and Yukseler (2022) used the Euler-Bernoulli beam theory to analyze the post- and snap-buckling characteristics of beams with initial defects under uniform loading. Andraju *et al*. (2021) illustrated the effect of bending loads on the snap-buckling behaviors of carbon fiber plates. Babaei and Eslami (2021) used the HSDT to study the nonlinear snap-buckling and vibration characteristics of FG cylindrical panels. Babaei and Eslami (2020) used the HSDT to discuss the effect of elastic foundation on nonlinear snap-buckling and vibration behaviors of FG porous curved pipes. Damanpack *et al.* (2018) discussed the snap-buckling characteristics of NiTi tubes using the iterative method. Sano and Wada (2018) studied the snap-buckling behavior of elastic belt with asymmetric restraint by numerical analysis.

In view of the previous literatures review, we can find that although the literatures on the analysis of doubly curved shell seem very rich, there is no work regarding the nonlinear bending of GPLRMF doubly curved shells with initial geometric imperfections. Because the derivation and solution of the formulas are very complex, the mechanism of nonlinear bending of doubly curved shells with geometric imperfections has not been clearly researched at present. In addition, the effects of parameters such as porosity coefficient, geometric imperfections, graphene mass fraction, graphene and pore distribution type on the vibration and bending behavior are described in detail.

2. Formulation

Fig. 1 shows the establishment of doubly curved shell coordinate system. In the figure, *a*, *b* and *h* represent the length, width and thickness of doubly curved shell, meanwhile, considering the longitudinal and transitional radius of curvature R_x and R_y. This paper analyzes the nonlinear bending response of shell under the same external environment. And three types of porosity and GPLs distribution are considered. What is more, assuming the material properties of GPLRMF shells (Poisson's ratio μ, mass density ρ and effective elastic modulus E) uniformly distributed along the thickness, which has the same expression forms as existing works (Wang *et al.* 2019, Yang *et al*. 2017, Chai and Wang 2022, She *et al.* 2025, Li and She 2025a, b, Zhang and She 2024, Zhang *et al*. 2024).

$$
\begin{aligned}
E(z)&=\begin{cases} E^{\#}\left[1-\mathrm{e}_1\cos(\pi z/h)\right], & (\text{Porosity-I})\\ E^{\#}\left\{1-\mathrm{e}_2\left[1-\cos(\pi z/h)\right]\right\}, & (\text{Porosity-II})\\ E^{\#}\mathrm{e}_3, & (\text{Porosity-III})\end{cases}\\
\rho(z)&=\begin{cases} \rho^{\#}\left[1-\mathrm{e}_{m1}\cos(\pi z/h)\right], & (\text{Porosity-I})\\ \rho^{\#}\left\{1-\mathrm{e}_{m2}\left[1-\cos(\pi z/h)\right]\right\}, & (\text{Porosity-II})\\ \rho^{\#}\mathrm{e}_{m3}, & (\text{Porosity-III})\end{cases}\\
\mu(z)&=\mu^{\#}
\end{aligned}
\tag{1}
$$

The definitions of these symbols $E^{\#}\mu^{\#}$, and $\rho^{\#}$ the same as our previous work (She and Ding 2023). According to the Halpin-Tsai micromechanical model (Wang *et al.* 2019, Yang *et al*. 2017).

$$
\begin{aligned}
E^{\#}&=\tfrac{3}{8}\tfrac{1+\zeta_L\eta_L V_{GPL}}{1-\eta_L V_{GPL}}\times E_M+\tfrac{5}{8}\tfrac{1+\zeta_W\eta_W V_{GPL}}{1-\eta_W V_{GPL}}\times E_M\\
\rho^{\#}&=\rho_{GPL}V_{GPL}+\rho_M\left(1-V_{GPL}\right)\\
\mu^{\#}&=\mu_{GPL}V_{GPL}+\mu_M\left(1-V_{GPL}\right)
\end{aligned}
\tag{2}
$$

Here, $\eta_L=\frac{(E_{GPL}/E_M)-1}{(E_{GPL}/E_M)+2(l_{GPL}/h_{GPL})}$, $\eta_W=\frac{(E_{GPL}/E_M)-1}{(E_{GPL}/E_M)+2(w_{GPL}/h_{GPL})}$, V_{GPL} refers to GPLs volume fraction, using $\frac{E(z)}{E_c}=\left[\frac{\rho(z)}{\rho_c}\right]^2$, then, we have (Song *et al*. 2024)

$$
\begin{cases}
1-e_{\mathrm{m1}}\cos(\pi z/h)=\sqrt{1-e_1\cos(\pi z/h)}\\
1-e_{\mathrm{m2}}\left[1-\cos(\pi z/h)\right]=\sqrt{1-e_2\left[1-\cos(\pi z/h)\right]}\\
e_{\mathrm{m3}}=\sqrt{e_3}
\end{cases}
\tag{3}
$$

Due to the fact that (Fan and She 2025)

$$
\int_0^{\frac{h}{2}}\sqrt{1-e_1\cos(\pi z/h)}dz=\int_0^{\frac{h}{2}}\sqrt{1-e_2\left[1-\cos(\pi z/h)\right]}dz=\int_0^{\frac{h}{2}}\sqrt{e_3}dz
\tag{4}
$$

In current paper, we consider three GPLs distributions, then we have (She *et al*. 2025, Li and She 2025a, b)

$$
V_{GPL}=\begin{cases} Si_1\left[1-\cos(\pi z/h)\right], & (\text{GPL-A})\\ Si_2\cos(\pi z/h), & (\text{GPL-B})\\ Si_3, & (\text{GPL-C})\end{cases}
\tag{5}
$$

These relevant mass fraction parameters, which can be obtained from the Refs. (Chai and Wang 2022).

By considering initial geometric imperfections (Cai and She 2025, Gan and She 2024, 2025, She and He 2025, Cheng and She 2024), using Reddy's HSDT, the displacement field can be given as (She and Ding 2023)

$$
\begin{aligned}
\mathrm{U}_1(x,y,z)&=u(x,y)-z\varphi_x-c_1z^3(\varphi_x+\frac{\partial w}{\partial x})\\
\mathrm{U}_2(x,y,z)&=v(x,y)-z\varphi_y-c_1z^3(\varphi_y+\frac{\partial w}{\partial y})\\
\mathrm{U}_3(x,y,z)&=w(x,y)+w_1(x,y)
\end{aligned}
\tag{6}
$$

In which, $c_1=4/(3h^2)$. At this point, the geometric equation can be expressed as

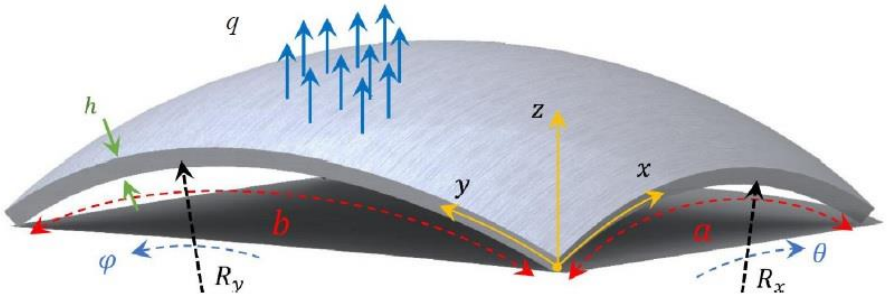

(a) A doubly curved shell

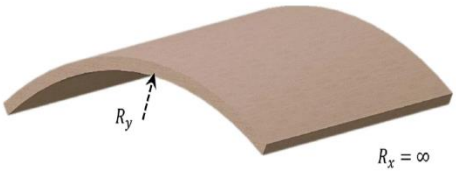

(b) Cylindrical shell

(c) Ellipsoidal shell

(d) Elliptical shell

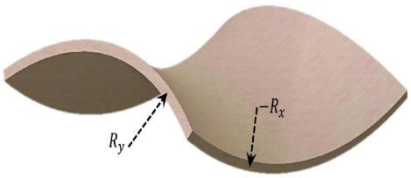

(e) Hyperbolic shell

Fig. 1 The sketch of doubly curved shells (Modified from Khaniki and Ghayesh 2023)

$$\begin{aligned}
\varepsilon_x &= \varepsilon_x^0 + z\kappa_x^1 + z^3\kappa_x^3 \\
\varepsilon_y &= \varepsilon_y^0 + z\kappa_y^1 + z^3\kappa_y^3 \\
\gamma_{xy} &= \gamma_{xy}^0 + z\kappa_{xy}^1 + z^3\kappa_{xy}^3 \\
\gamma_{xz} &= \gamma_{xz}^0 + z^2\gamma_{xz}^2 \\
\gamma_{yz} &= \gamma_{yz}^0 + z^2\gamma_{yz}^2
\end{aligned} \tag{7}$$

In which

$$\begin{aligned}
&\varepsilon_x^0 = \frac{\partial u}{\partial x} - \frac{w}{R} + \frac{1}{2}\left(\frac{\partial w}{\partial x}\right)^2 + \frac{\partial w}{\partial x}\frac{\partial w_1}{\partial x} \\
&\varepsilon_y^0 = \frac{\partial v}{\partial y} - \frac{w}{R} + \frac{1}{2}\left(\frac{\partial w}{\partial y}\right)^2 + \frac{\partial w}{\partial y}\frac{\partial w_1}{\partial y} \\
&\gamma_{xy}^0 = \frac{\partial u}{\partial y} + \frac{\partial v}{\partial x} + \frac{\partial w}{\partial x}\frac{\partial w}{\partial y} + \frac{\partial w}{\partial x}\frac{\partial w_1}{\partial y} + \frac{\partial w}{\partial y}\frac{\partial w_1}{\partial x} \\
&\kappa_x^1 = \frac{\partial \varphi_x}{\partial x}, \kappa_y^1 = \frac{\partial \varphi_y}{\partial y}, \kappa_{xy}^1 = \frac{\partial \varphi_x}{\partial y} + \frac{\partial \varphi_y}{\partial x}, \\
&\begin{pmatrix} \kappa_x^3 \\ \kappa_y^3 \\ \kappa_{xy}^3 \end{pmatrix} = -c_1 \begin{pmatrix} \dfrac{\partial \varphi_x}{\partial x} \\ \dfrac{\partial \varphi_y}{\partial y} \\ \dfrac{\partial \varphi_x}{\partial y} + \dfrac{\partial \varphi_y}{\partial x} \end{pmatrix}, \\
&\begin{pmatrix} \gamma_{xz}^0 \\ \gamma_{yz}^0 \end{pmatrix} = \begin{pmatrix} \varphi_x + \dfrac{\partial w}{\partial x} \\ \varphi_y + \dfrac{\partial w}{\partial y} \end{pmatrix}, \begin{pmatrix} \gamma_{xz}^2 \\ \gamma_{yz}^2 \end{pmatrix} = c_2 \begin{pmatrix} \varphi_x + \dfrac{\partial w}{\partial x} \\ \varphi_y + \dfrac{\partial w}{\partial y} \end{pmatrix}.
\end{aligned} \tag{8}$$

In which, c_2=3c_1. According to Hooke's Law, the relationship between stress and strain can be written as

$$\begin{bmatrix} \sigma_x \\ \sigma_y \\ \sigma_{xz} \\ \sigma_{yz} \\ \sigma_{xy} \end{bmatrix} = \begin{bmatrix} Q_{11} & Q_{12} & 0 & 0 & 0 \\ Q_{12} & Q_{22} & 0 & 0 & 0 \\ 0 & 0 & Q_{44} & 0 & 0 \\ 0 & 0 & 0 & Q_{55} & 0 \\ 0 & 0 & 0 & 0 & Q_{66} \end{bmatrix} \begin{bmatrix} \varepsilon_x \\ \varepsilon_y \\ \gamma_{xz} \\ \gamma_{yz} \\ \gamma_{xy} \end{bmatrix} \tag{9}$$

In which

$$\begin{aligned}
&Q_{11} = Q_{22} = \frac{E(z)}{1-\nu^2},\ Q_{66} = \frac{E(z)}{2(1+\nu)},\ Q_{12} = \frac{\nu E(z)}{1-\nu^2}, \\
&Q_{55} = Q_{44} = Q_{66}
\end{aligned} \tag{10}$$

The expression for the relationship between internal force and stress is

$$\begin{aligned}
&\begin{bmatrix} N_x \\ N_y \\ N_{xy} \end{bmatrix} = \int_{-h/2}^{h/2} \begin{bmatrix} \sigma_x \\ \sigma_y \\ \sigma_{xy} \end{bmatrix} dz, \begin{bmatrix} M_x \\ M_y \\ M_{xy} \end{bmatrix} = \int_{-h/2}^{h/2} z \begin{bmatrix} \sigma_x \\ \sigma_y \\ \sigma_{xy} \end{bmatrix} dz, \\
&\begin{bmatrix} T_x \\ T_y \\ T_{xy} \end{bmatrix} = \int_{-h/2}^{h/2} z^3 \begin{bmatrix} \sigma_x \\ \sigma_y \\ \sigma_{xy} \end{bmatrix} dz, \begin{bmatrix} Q_x \\ Q_y \end{bmatrix} = \int_{-h/2}^{h/2} \begin{bmatrix} \sigma_{xz} \\ \sigma_{yz} \end{bmatrix} dz, \\
&\begin{bmatrix} S_x \\ S_y \end{bmatrix} = \int_{-h/2}^{h/2} z^2 \begin{bmatrix} \sigma_{xz} \\ \sigma_{yz} \end{bmatrix} dz.
\end{aligned} \tag{11}$$

By applying the Hamiltonian variational principle, the vibration equation can be obtained.

$$\frac{\partial N_x}{\partial x}+\frac{\partial N_{xy}}{\partial y}=0 \tag{12}$$

$$\frac{\partial N_{xy}}{\partial x}+\frac{\partial N_y}{\partial y}=0 \tag{13}$$

$$\begin{aligned}&\frac{\partial Q_x}{\partial x}+\frac{\partial Q_y}{\partial y}+c_2\left(\frac{\partial S_x}{\partial x}+\frac{\partial S_y}{\partial y}\right)+c_1\left(\frac{\partial^2 T_x}{\partial x^2}+2\frac{\partial T_{xy}}{\partial x\partial y}+\frac{\partial^2 T_y}{\partial y^2}\right)\\&+\frac{N_x}{R_x}+\frac{N_y}{R_y}+N_x\frac{\partial^2 w}{\partial x^2}+2N_{xy}\frac{\partial^2 w}{\partial x\partial y}+N_y\frac{\partial^2 w}{\partial y^2}\\&-P\frac{\partial^2 w}{\partial x^2}+q=0,\end{aligned} \tag{14}$$

$$\frac{\partial M_x}{\partial x}+\frac{\partial M_{xy}}{\partial y}-Q_x+c_2S_x-c_1\left(\frac{\partial T_x}{\partial x}+\frac{\partial T_{xy}}{\partial y}\right)=0, \tag{15}$$

$$\frac{\partial M_{xy}}{\partial x}+\frac{\partial M_y}{\partial y}-Q_y+c_2S_y-c_1\left(\frac{\partial T_{xy}}{\partial x}+\frac{\partial T_y}{\partial y}\right)=0. \tag{16}$$

Using Eqs. (6)-(11), Eqs. (12)-(16) can be further written as

$$\begin{aligned}&L_{11}(u)+L_{12}(v)+L_{13}(w)+L_{14}(w^2)+L_{15}(\varphi_x)+L_{16}(\varphi_y)\\&=0,\end{aligned} \tag{17}$$

$$\begin{aligned}&L_{21}(u)+L_{22}(v)+L_{23}(w)+L_{24}(w^2)+L_{25}(\varphi_x)+L_{26}(\varphi_y)\\&=0,\end{aligned} \tag{18}$$

$$\begin{aligned}&L_{31}(u)+L_{32}(v)+L_{33}(w)+L_{34}(w^2)+L_{35}(w^3)\\&+L_{36}(\varphi_x)+L_{37}(\varphi_y)+L_{38}(u,w)+L_{39}(v,w)+L_{310}(\varphi_x,w)\\&+L_{311}(\varphi_y,w)+q=0,\end{aligned} \tag{19}$$

$$\begin{aligned}&L_{41}(u)+L_{42}(v)+L_{43}(w)+L_{44}(w^2)+L_{45}(\varphi_x)\\&+L_{46}(\varphi_y)=0,\end{aligned} \tag{20}$$

$$\begin{aligned}&L_{51}(u)+L_{52}(v)+L_{53}(w)+L_{54}(w^2)+L_{55}(\varphi_x)\\&+L_{56}(\varphi_y)=0.\end{aligned} \tag{21}$$

These symbols appeared in Eqs. (17)-(21) are defined in Ref. (She and Ding 2023).

Considering the simply supported boundary condition (SSSS), the clamped-clamped-simply-simply supported boundary condition (CCSS), the clamped supported boundary condition (CCCC), the following displacement type function is adopted (Melaibari *et al*. 2022, She and Ding 2023)

$$\begin{aligned}&\{u,\varphi_x\}=\sum_{m=1}^{\infty}\sum_{n=1}^{\infty}\{U_{mn},(\Phi_x)_{mn}\}\frac{\partial X_m(x)}{\partial x}\gamma_n(y),\\&\{v,\varphi_y\}=\sum_{m=1}^{\infty}\sum_{n=1}^{\infty}\{V_{mn},(\Phi_y)_{mn}\}X_m(x)\frac{\partial\gamma_n(y)}{\partial y},\\&\{w,w_1\}=\sum_{m=1}^{\infty}\sum_{n=1}^{\infty}\{W_{mn},(W_1)_{mn}\}X_m(x)\gamma_n(y).\end{aligned} \tag{22}$$

For SSSS (Melaibari *et al.* 2022)

$$\{X_m(x),\gamma_n(y)\}=\left\{\sin\left(\frac{\pi mx}{a}\right),\sin\left(\frac{\pi ny}{b}\right)\right\} \tag{23}$$

For CCSS (Melaibari *et al.* 2022)

$$\{X_m(x),\gamma_n(y)\}=\left\{\sin^2\left(\frac{\pi mx}{a}\right),\sin\left(\frac{\pi ny}{b}\right)\right\} \tag{24}$$

For CCCC (Melaibari *et al*. 2022)

$$\{X_m(x),\gamma_n(y)\}=\left\{\sin^2\left(\frac{\pi mx}{a}\right),\sin^2\left(\frac{\pi ny}{b}\right)\right\} \tag{25}$$

In Eqs. (22)-(25), (m, n) are the axial wave number and circumferential half wave number. For the static problem, only the first-order mode is the valid mode, which means m=n=1. Substitute Eqs. (22)-(25) into Eqs. (17)-(21), and then use the Galerkin method to process them. Transform the partial differential equation into an ordinary differential equation, and then obtain six ordinary differential equations in the form of

$$l_{11}U+l_{12}V+l_{13}W+l_{14}W^2+l_{15}\Phi_x+l_{16}\Phi_y=0, \tag{26}$$

$$\begin{aligned}&l_{21}U+l_{22}V+l_{23}W+l_{24}W^2+l_{25}\Phi_x+l_{26}\Phi_y=0,\\&l_{31}U+l_{32}V+l_{33}W+l_{34}W^2+l_{35}W^3+l_{36}\Phi_x+l_{37}\Phi_y\\&+l_{38}UW+l_{39}VW+l_{310}\Phi_xW+l_{311}\Phi_yW+q=0,\\&l_{41}U+l_{42}V+l_{43}W+l_{44}W^2+l_{45}\Phi_x+l_{46}\Phi_y=0,\\&l_{51}U+l_{52}V+l_{53}W+l_{54}W^2+l_{55}\Phi_x+l_{56}\Phi_y=0.\end{aligned}$$

The definitions of these symbols $E^{\#}\mu^{\#}$, and $\rho^{\#}$ are the same as our previous work (She and Ding 2023). By eliminating U, V, Φ_x and Φ_y in Eq. (27), we can get the expression between the load and deflection.

$$I_1\frac{d^2W}{dt^2}+F_1W+F_2W^2+F_3W^3=\lambda_q \tag{27}$$

Finally, Eq. (28) can be solved using the Newton-Raphson approach.

3. Numerical analyses

In the paper and in the following research, the adopted material is the same as our previous paper (She and Ding 2023). To prove the accuracy and feasibility of the method proposed in this study, this paper compares the result which is obtained by using FSDT (See Fig. 2). Through comparison, we can find that the two curves are close to fitting, so that the method proposed in this paper (Reddy's HSDT) is feasible.

Fig. 3 studies the effect of GPLs distribution type on the snap-buckling behavior of GPLRMF shells. Three distribution types are considered. On the one hand, we can see from the Fig.3 that the snap-buckling will occur under the three types, and the GPL-A curve is always above the three curves, the GPL-B curve is below, and the GPL-C curve is between the two. On the other hand, by comparing

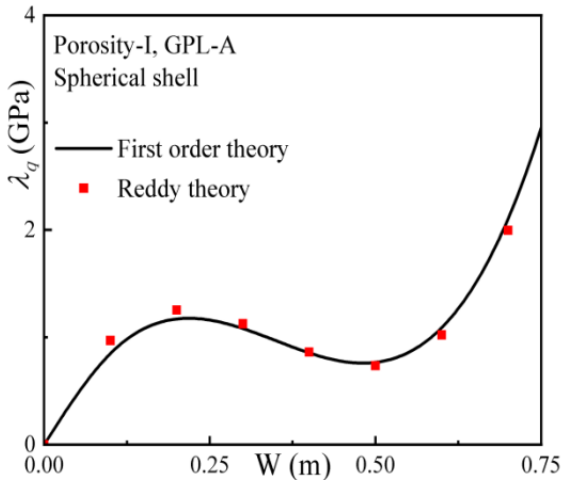

Fig. 2 Comparative study (e_1=0.*Wgpl*=1%, *W*1=0.4, *a*=*b*=2 m, *h*=0.05 m, *Rx*=*Ry*=2 m, *Ph* = 3.5 GPa)

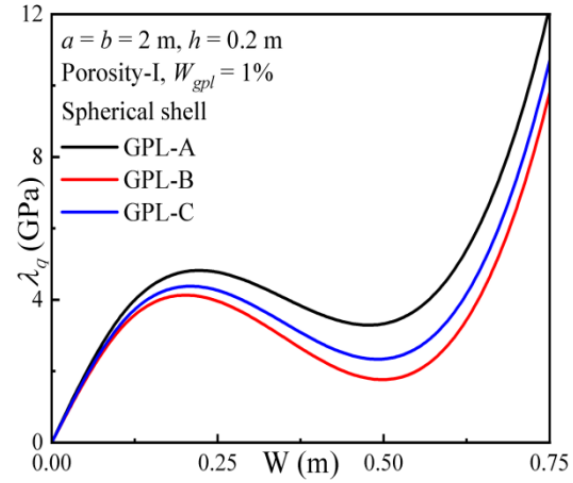

Fig. 3 Effect of GPLs distribution types (e_1=0.2, W_1 =0.4, *Ph* = 3.5 GPa, e_1=0.2, W_{gpl}=1%, W_1=0.4, *a*=*b*=2 m, *h*=0.2 m, *Rx*=*Ry*=2 m, Porosity-I)

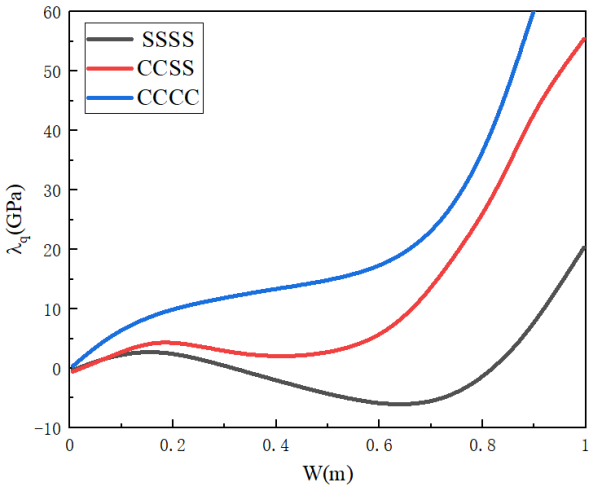

Fig. 4 Effect of different boundary conditions (W_{gpl}=1%, W_1=0.6, *a*=*b*=2 m, *h*=0.2 m, *Ph* = 3 GPa, Porosity-I, GPL-A, *Rx*=-*Ry*=2 m)

the change paths of the three curves, we can get that GPL-B has the maximum buckling strength, followed by GPL-C, and finally GPL-A. Therefore, we can obtain the information that is the buckling strength is closely related to the distribution type of graphene. For the natural frequency, GPL-A>GPL-C>GPL-B.

Fig. 4 plots the snap-buckling response of the doubly curved shell structures under different boundary conditions (including SSSS, CCSS and CCCC). As seen, compared with the case of CCCC shell, the SSSS shell is more prone to snap-buckling, followed by the CCSS shell. This is because the CCCC can provide more constraint conditions, making the structure more difficult to snap-buckling.

The effect of GPLs mass fraction on the disturbance-load curve of GPLRMF shell is shown in Fig. 5. It is not difficult to see that the mass fraction of graphene has a significant effect on the snap-buckling behavior. When the disturbance is constant, the required external load will increase with the increase of the mass fraction of graphene. In other words, when the same disturbance is generated, the mass fraction of graphene is proportional to the load applied on the body. This is because the strength of graphene is very high, thus, the greater the mass fraction of graphene, the stronger the resistance to deformation.

Fig. 6 discusses the influence of pre-stressed *Ph* on the snap-buckling characteristics of GPLRMF shells. It is obvious to see that the snap-buckling phenomenon will occur regardless of whether there is pre-stressed. And with the increase of Ph, the disturbance-load curve will move down as a whole. When *Ph* =4 GPa, the disturbance-load curve is at the bottom of the whole, followed by *Ph* =2GPa and *Ph* =0 GPa. In addition, there is an obvious phenomenon that the buckling strength will increase with the increase of *Ph*. This is because prestress can significantly improve the service performance of the structure.

Fig.7 analyzes the influence of pore distribution type on the snap-buckling characteristics of GPLRMF shells. The three distribution types are considered. We can find that when the same load is applied, the Porosity-II reaches the first and second limit positions at the earliest, followed by Porosity-II and Porosity-I, and the D-value between the two limit positions of Porosity-II is the largest, which is representing the maximum bucking strength. Therefore, the type of pore distribution has a significant impact on the snap-buckling behavior.

Fig. 8 discusses the effect of geometric imperfections W_1 on the snap-buckling behavior of GPLRMF shell. It can be seen from the figure that when W_1=0.2, snap-buckling will occur. On the contrary, when W_1=0.0, the load is a monotonically increasing function of deflection, and snap-buckling will not occur at this time. Based on the above analysis, it can be concluded that the stability is related to the value of W_1. When the value of W_1 is small enough (for example, W_1=0), the disturbance is a monotonically increasing function of the load. At this time, snap-buckling will not occur; When W_1 is relatively large (such as W_1=0.2), GPLRMF shells are prone to snap-buckling behavior under external load, because the existence of geometric imperfections will significantly reduce the

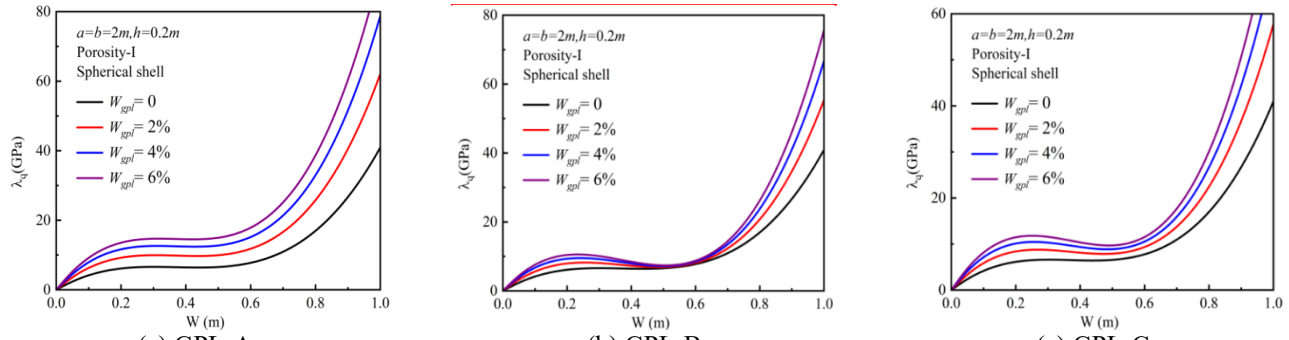

(a) GPL-A (b) GPL-B (c) GPL-C

Fig. 5 Effect of mass GPLs fraction (W_{gpl}=1%, W_1=0.6, Ph = 3 GPa, a=b=2 m, h=0.2 m, Rx=Ry=2 m, Porosity-I, SSSS)

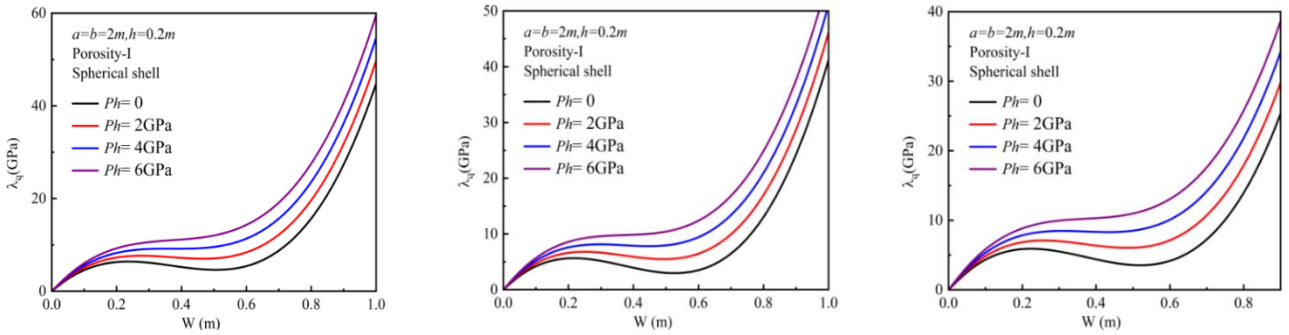

(a) GPL-A (b) GPL-B (c) GPL-C

Fig. 6 Effect of prestress (W_{gpl}=1%, W_1=0.6, Ph=3 GPa, a=b=2 m, h=0.2 m, Rx=Ry=2 m, Porosity-I, GPL-A, SSSS)

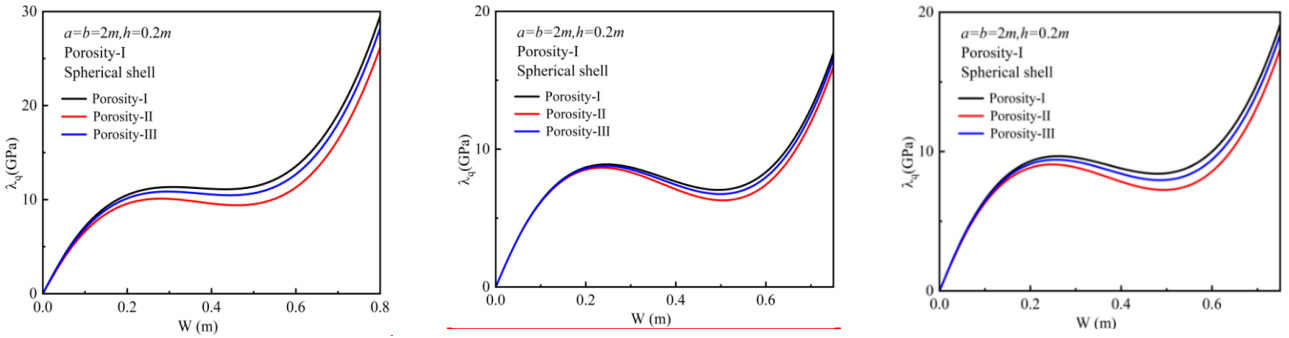

(a) GPL-A (b) GPL-B (c) GPL-C

Fig. 7 Effect of pore distribution types (e_1=0.4, W_1 =0.6, W_{gpl}=3%, Ph = 3 GPa, a=b=2 m, h=0.2 m, Rx=Ry=2 m, Porosity-I, GPL-A, SSSS)

Young's modulus and tensile strength of graphene, and the mechanical properties of graphene will decline with the increase of the number of imperfections.

Fig. 9 discusses the snap-buckling response of four different structures under the same external factor. We can intuitively see that when the external factors are fixed, the snap-buckling characteristics of different structures are different. The disturbance-load curve of hyperbolic is a monotonically increasing function, so it is difficult to occur snap-buckling; Compared with the hyperbolic shell, the spherical shell is more prone to snap-buckling, followed by the ellipsoid, and finally the cylindrical shell. That is to say, whether the object will snap-buckling is closely related to its own structure. This is because the bearing capacity of different structures is different, so that the resistance to deformation is also different.

Fig. 10 studies the effect of pore coefficient e_1 on the snap-buckling behavior of GPLRMF shell. It can be intuitively seen from the figure that the shell will have obvious snap-buckling behavior regardless of whether the pores exist. That is, with the increase of the disturbance, the disturbance-load curve has monotonically increased and decreasing intervals, and we call the difference between the two adjacent extreme values as the buckling strength, which means the ability to resist small plastic deformation. In addition, we can also find that, the external load required for the shell with large porosity coefficient is far less than that for the shell with small porosity coefficient. In other words, when e_1=0, the external load required for the shell is the largest, and when e_1=0.6, the external load applied on the shell is the smallest. Finally, we can see that with the

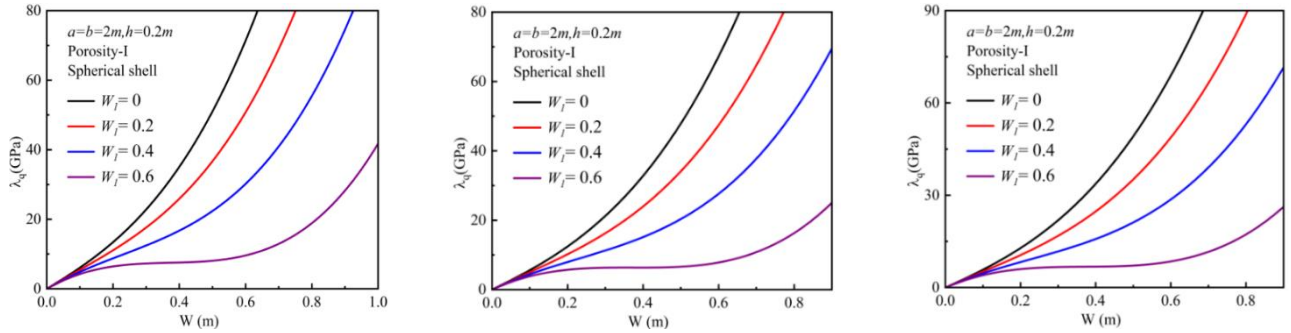

(a) GPL-A (b) GPL-B (c) GPL-C

Fig. 8 Effect of geometric imperfections W_1(e_1=0.4, W_1 =0.6, W_{gpl}=3%, Ph =3 GPa, a=b=2 m, h=0.2 m, Rx=Ry=2 m, Porosity-I, GPL-A, SSSS)

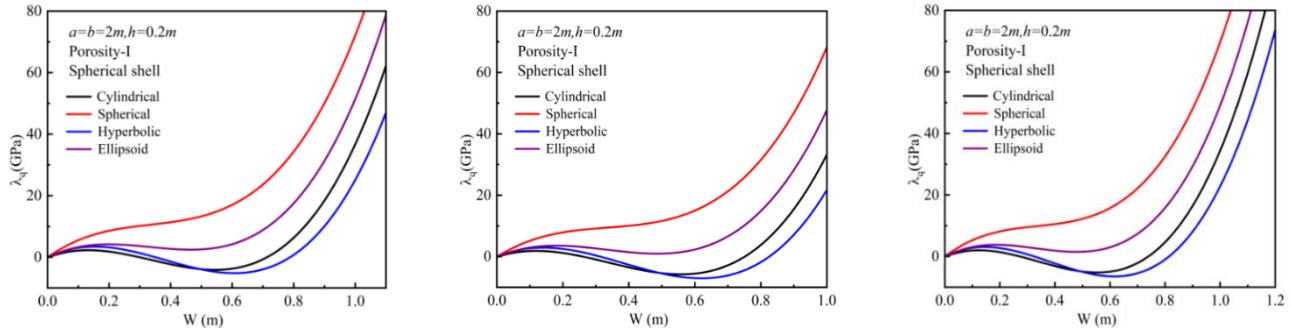

(a) GPL-A (b) GPL-B (c) GPL-C

Fig. 9 Effect of different shell types (e_1=0.2, W_{gpl}=1%, W_1 =0.55, Ph=3 Gpa, SSSS), in which for spherical shell Rx=Ry=2 m, for cylindrical shell Rx=∞,Ry=+2m, for hyperbolic shell Rx=-Ry=2m, for ellipsoid shell Rx=0.5Ry=2 m

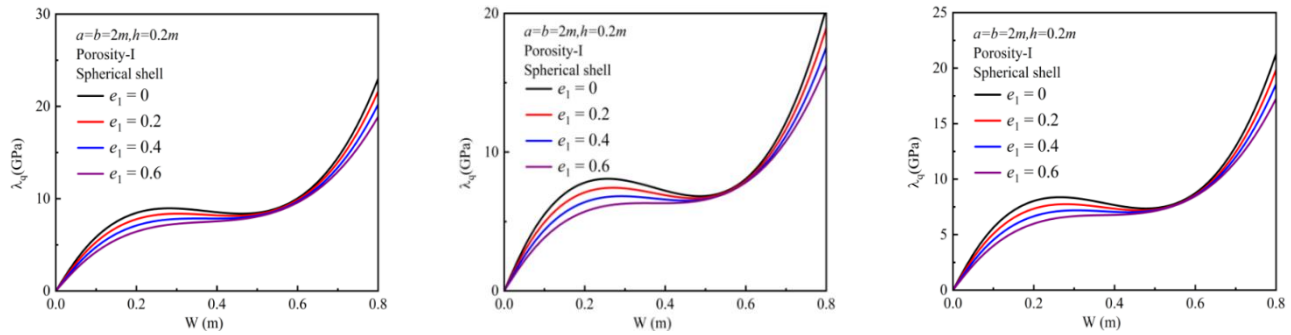

(a) GPL-A (b) GPL-B (c) GPL-C

Fig. 10 Effect of pore coefficient values (W_{gpl}=1%, W_1=0.6, a=b=2 m, h=0.2 m, Ph = 3 GPa, Porosity-I, GPL-A, Rx=Ry=2 m, SSSS)

increase of e_1, the buckling strength decreases. This is because the larger the porosity coefficient, the more the through-holes, the lower the strength.

4. Conclusions

The current work mainly focuses on the analysis of the snap-buckling response of GPLRMF doubly curved shell. Firstly, based on Euler-Lagrange principle and Reddy's HSDT, the motion control equation is obtained. Secondly, the Galerkin method is used to derive the nonlinear ordinary differential equations. Finally, the relationship between the disturbance and the load is obtained. Meanwhile, we have systematically researched the parameters to fully interpret the effects of the introduced parameters on the snap-buckling behavior of GPLRMF doubly curved shell based on Newton-Raphson approach. The summaries are as follows:

(1) With the increase of e_1, the buckling strength of GPLRMF doubly curved shells decreases.

(2) The distribution type of GPL and pore have significant influence on the snap-buckling characteristics. the GPL-B has the maximum buckling strength, followed by GPL-C and GPL-A. Similarly, the Porosity-II has the largest buckling strength, followed by Porosity-III and

Porosity-I.

(3) The W_{gpl} and prestress have different effects on the snap-buckling characteristics. When the disturbance is constant, the required load will increase with the increase of W_{gpl}. However, the greater the prestress, the smaller the required load.

(4) When W_1=0.0, the GPLRMF doubly curved shells will not have snap-buckling behavior. When W_1 increases to a certain value (W_1=0.2), the disturbance -load curve will show snap-buckling characteristics.

(5) Compared with the hyperbolic shell, the spherical shell is more prone to snap-buckling, followed by the ellipsoid, and finally the cylindrical shell.

(6) Compared CCCC, the SSSS shell is more prone to snap-buckling, followed by the CCSS shell, which is because the CCCC can provide more constraint conditions.

References

Aminipour, H. and Emam, S. (2022), "Snapthrough response of doubly curved laminated shells for pressure sensing applications", *Meccanica*, **57**(3), 577-597. https://doi.org/10.1007/s11012-021-01451-y.

Arefi, M. and Amabili, M. (2021), "A comprehensive electro-magneto-elastic buckling and bending analyses of three-layered doubly curved nanoshell, based on nonlocal three-dimensional theory", *Compos. Struct*., **257**, 113100. https://doi.org/10.1016/j.compstruct.2020.113100.

Aminipour, H., Janghorban, M. and Civalek, O. (2020), "Analysis of functionally graded doubly-curved shells with different materials via higher order shear deformation theory", *Compos. Struct*., **251**, 112645. https://doi.org/10.1016/j.compstruct.2020.112645.

Arefi, M., Bidgoli, E.M.R. and Civalek, O. (2022), "Bending response of FG composite doubly curved nanoshells with thickness stretching via higher-order sinusoidal shear theory", *Mech. Based. Des. Struc*., **50**(7), 2350-2378. https://doi.org/10.1080/15397734.2020.1777157.

Abbasi, A., Sano, T.G., Yan, D. and Reis, P.M. (2023), "Snap buckling of bistable beams under combined mechanical and magnetic loading", *Philos. T. R. Soc. A*., **381**(2244), 20220029. https://doi.org/10.1098/rsta.2022.0029.

Atacan, A.T. and Yukseler, R.F. (2022), "Snap-buckling and post-buckling analyses of fixed supported beams having initially small circular imperfection under the effect of uniformly distributed vertical load", *J. Fac. Eng. Archit. Gaz*., **37**(2), 1091-1102. https://doi.org/10.17341/gazimmfd.845996.

Andraju, L.B., Ramji, M. and Raju, G. (2021), "Snap-buckling and failure studies on CFRP laminate with an embedded circular delamination under flexural loading", *Compos. Part. B-Eng*., **214**, 108739. https://doi.org/10.1016/j.compositesb.2021.108739.

Babaei, H. (2022), "Free vibration and snap-through instability of FG-CNTRC shallow arches supported on nonlinear elastic foundation", *Appl. Math. Comput*., **413**, 126606. https://doi.org/10.1016/j.amc.2021.126606.

Babaei, H. and Eslami, M.R. (2021a), "Nonlinear analysis of thermal-mechanical coupling bending of FGP infinite length cylindrical panels based on PNS and NSGT", *Appl. Math. Model*., **91**, 1061-1080. https://doi.org/10.1016/j.apm.2020.10.004.

Babaei, H. and Eslami, M.R. (2021b), "Nonlinear analysis of thermal-mechanical coupling bending of clamped FG porous curved micro-tubes", *J. Therm. Stresses*, **44**(4), 409-432. https://doi.org/10.1080/01495739.2020.1870417.

Cai, Y. and She, G.L. (2025), "Nonlinear dynamic response of magneto-electro-elastic cylindrical shells subjected to moving load", *Mech. Adv. Mater. Struct*., https://doi.org/10.1080/15376494.2025.2463090.

Chai, Q.D. and Wang, Y.Q. (2022), "Traveling wave vibration of graphene platelet reinforced porous joined conical-cylindrical shells in a spinning motion", *Eng. Struct*., **252**, 113718. https://doi.org/10.1016/j.engstruct.2021.113718.

Cheng, Y.H. and She, G.L. (2024), "Nonlinear low-velocity impact of graphene platelet-reinforced metal foam beam with geometrical imperfection", *Steel Compos. Struct*., **52**(6), 609-620. https://doi.org/10.12989/scs.2024.52.6.609.

Dai, H.M. and Safarpour, H. (2021), "Frequency and thermal buckling information of laminated composite doubly curved open nanoshell", *Adv. Nano. Res*., **10**(1), 1-14. https://doi.org/10.12989/anr.2021.10.1.001.

Damanpack, A.R., Bodaghi, M. and Liao, W.H. (2018), "Snap buckling of NiTi tubes", *Int. J. Solids. Struct*., **146**, 29-42. https://doi.org/10.1016/j.ijsolstr.2018.03.016.

Fan, Y.H. and She, G.L. (2025) "Nonlinear transient response of graphene platelets reinforced metal foams beam considering initial geometrical imperfection and viscoelastic elastic foundation", *Comput. Concrete*, **35**(1), 59-70. https://doi.org/10.12989/cac.2025.35.1.059.

Gan, L.L. and She, G.L. (2024), "Nonlinear transient response of magneto-electro-elastic cylindrical shells with initial geometric imperfection", *Appl. Math. Modell*., **132**, 166-186. https://doi.org/10.1016/j.apm.2024.04.049.

Gan, L.L. and She, G.L. (2025), "Nonlinear combined resonance of magneto-electro-elastic plates", *Eur. J. Mech. – A Solids*, **109**, 105492. https://doi.org/10.1016/j.euromechsol.2024.105492.

Gao, K., Gao, W., Chen, D. and Yang, J. (2018), "Nonlinear free vibration of functionally graded graphene platelets reinforced porous nanocomposite plates resting on elastic foundation", *Compos. Struct*., **204**, 831-846. https://doi.org/10.1016/j.compstruct.2018.08.013.

Huang, S.X. and Qiao, P.Z. (2020), "A new semi-analytical method for nonlinear stability analysis of stiffened laminated composite doubly-curved shallow shells", *Compos. Struct*., **251**, 112526. https://doi.org/10.1016/j.compstruct.2020.112526.

Hoang, V.N.V., Tien, N.D., Ninh, D.G., Thang, V.T. and Truong, D.V. (2021), "Nonlinear dynamics of functionally graded graphene nanoplatelet reinforced polymer doubly-curved shallow shells resting on elastic foundation using a micromechanical model", *J. Sandw. Struct. Mater*., **23**(7), 3250-3279. https://doi.org/10.1177/1099636220926650.

Houmat, A. (2008), "Large amplitude free vibration of shear deformable laminated composite annular sector plates by a sector p-element", *Int. J. Nonlinear Mech*., **43**(9), 834-843. https://doi.org/10.1016/j.ijnonlinmec.2008.05.007.

Jing, Z., Li, X., Sun, Q., Liang, K., Zhang, Y.J. and Duan, L. (2022), "A 2D-sampling optimization method for buckling layup design of doubly-curved laminated composite shallow shells", *Compos. Struct*., **297**, 115934. https://doi.org/10.1016/j.compstruct.2022.115934.

Karimiasl, M., Ebrahimi, F. and Mahesh, V. (2021), "Postbuckling analysis of piezoelectric multiscale sandwich composite doubly curved porous shallow shells via Homotopy Perturbation Method", *Eng. Comput-Germany*., **37**(1), 561-577. https://doi.org/10.1007/s00366-019-00841-x.

Karami, B. and Shahsavari, D. (2020), "On the forced resonant vibration analysis of functionally graded polymer composite doubly-curved nanoshells reinforced with graphene-nanoplatelets", *Comput. Method. Appl. M*., **359**. https://doi.org/10.1016/j.cma.2019.112767.

Khaniki, H.B. and Ghayesh, M.H. (2023), "Highly nonlinear hyperelastic shells: Statics and dynamics", *Int. J. Eng. Sci*., **183**,

103794. https://doi.org/10.1016/j.ijengsci.2022.103794.

Kundu, C.K. and Sinha, P.K. (2007), "Post buckling analysis of laminated composite shells", *Compos. Struct*., **78**(3), 316-324. https://doi.org/10.1016/j.compstruct.2005.10.005.

Li, Y.P. and She, G.L. (2025a), "Nonlinear dynamic response of porous graphene platelets reinforced plates subjected to moving load considering initial geometrical imperfection", *J. Vib. Eng. Tech.*, **13**(1), 17. https://doi.org/10.1007/s42417-024-01651-2

Li, Y.P. and She, G.L. (2025b), "Nonlinear dynamic response of graphene platelets reinforced cylindrical shells under moving loads considering initial geometric imperfection", *Eng. Struct*., **323**, 119241. https://doi.org/10.1016/j.engstruct.2024.119241.

Liu, T., Li, Z.M. and Qiao, P.Z. (2021), "The closed-form solutions for buckling and postbuckling behaviour of anisotropic shear deformable laminated doubly-curved shells by matching method with the boundary layer of shell buckling", *Acta. Mech*., **232**(8), 3277-3303. https://doi.org/10.1007/s00707-021-02952-3.

Melaibari, A., Daikh, A.A., Basha, M., Abdalla, A.W., Othman, R., Almitani, K.H., Hamed, M.A., Abdelrahman, A, and Eltaher, M.A. (2022), "Free vibration of FG-CNTRCs nano-plates/shells with temperature-dependent properties", *Mathematics*, **10**(4), 583. https://doi.org/10.3390/math10040583.

Mirjavadi, S.S., Forsat, M., Yahya, Y.Z., Barati, M.R., Jayasimha, A.N. and Hamouda, A.M.S. (2020), "Porosity effects on post-buckling behavior of geometrically imperfect metal foam doubly-curved shells with stiffeners", *Struct. Eng. Mech*., **75**(6), 701-711. https://doi.org/10.12989/sem.2020.75.6.701.

Rezaee, S. and Yazdi, A.A. (2022), "Similarity conditions for predicting the effect of carbon nano-tubes on the non-linear frequency of laminated doubly curved shells", *Structures*, **46**, 1618-1625. https://doi.org/10.1016/j.istruc.2022.11.009.

Sano, T.G. and Wada, H. (2018), "Snap-buckling in asymmetrically constrained elastic strips", *Phys. Rev. E*., **97**(1), 013002. https://doi.org/10.1103/PhysRevE.97.013002.

Sharma, L.K., Grover, N., Purohit, A. and Sahoo, R. (2021), "A non-polynomial axiomatic framework for modelling and bending analysis of doubly curved spherical and cylindrical shells: An analytical solution", *P. I. Mech. Eng. L-J. Mat*., **235**(9), 2083-2099. https://doi.org/10.1177/14644207211023528.

Shahmohammadi, M.A., Abdollahi, P. and Salehipour, H. (2022), "Geometrically nonlinear analysis of doubly curved imperfect shallow shells made of functionally graded carbon nanotube reinforced composite (FG_CNTRC)", *Mech. Based. Des. Struc*., **50**(11), 3796-3820. https://doi.org/10.1080/15397734.2020.1822182.

She, G.L. and Ding, H.X. (2023), "Nonlinear primary resonance analysis of initially stressed graphene platelet reinforced metal foams doubly curved shells with geometric imperfection", *Acta Mech. Sin*., **39**, 522392. https://doi.org/10.1007/s10409-022-22392-x.

She, G.L. and He, Y.J. (2025), "Nonlinear thermal buckling of magneto-electro-thermal-elastic plates with geometric imperfection", *Struct. Eng. Mech*., **93**(2), 115-123. https://doi.org/10.12989/sem.2025.93.2.115.

She, G.L., Ma, Z.S., Li, C. and Eltaher, M.A. (2025), "Geometrically nonlinear transient response of graphene platelets reinforced metal foams arbitrary quadrilateral plates under blast load", *Thin Wall. Struct*., **210**, 113018. https://doi.org/10.1016/j.tws.2025.113018.

Song, J.P., She, G.L. and Eltaher, M.A. (2024), "Nonlinear vibrations of variable speed rotating graphene platelets reinforced blades subjected to combined parametric and forced excitation", *Thin Wall. Struct.*, **204**, 112283. https://doi.org/10.1016/j.tws.2024.112283.

Tornabene, F., Viscoti, M. and Dimitri, R. (2023), "Static analysis of anisotropic doubly-curved shell subjected to concentrated loads employing higher order layer-wise theories", *Cmes-Comp. Model. Eng*., **134**(2), 1393-1468. https://doi.org/10.32604/cmes.2022.022237.

Tornabene, F., Viscoti, M. and Dimitri, R. (2022), "Equivalent single layer higher order theory based on a weak formulation for the dynamic analysis of anisotropic doubly-curved shells with arbitrary geometry and variable thickness", *Thin. Wall. Struct*., **174**, 109119. https://doi.org/10.1016/j.tws.2022.109119.

Tornabene, F., Viscoti, M., Dimitri, R. and Aiello, M.A. (2021), "Higher order formulations for doubly-curved shell structures with a honeycomb core", *Thin. Wall. Struct*., **164**, 107789. https://doi.org/10.1016/j.tws.2021.107789.

Trinh, M.C. and Kim, S.E. (2019), "A three variable refined shear deformation theory for porous functionally graded doubly curved shell analysis", *Aerosp. Sci. Technol*., **94**, 105356. https://doi.org/10.1016/j.ast.2019.105356.

Vinh, P.V. and Tounsi, A. (2022), "Free vibration analysis of functionally graded doubly curved nanoshells using nonlocal first-order shear deformation theory with variable nonlocal parameters", *Thin. Wall. Struct*., **174**, 109084. https://doi.org/10.1016/j.tws.2022.109084.

Wang, Y., Xie, K., Fu, T. and Shi, C. (2019), "Vibration response of a functionally graded graphene nanoplatelet reinforced composite beam under two successive moving masses", *Compos. Struct*., **209**, 928-939. https://doi.org/10.1016/j.compstruct.2018.11.014.

Xu, X.Z., Karami, B. and Janghorban, M. (2021), "On the dynamics of nanoshells", *Int. J. Eng. Sci*., **158**, 103431. https://doi.org/ 10.1016/j.ijengsci.2020.103431.

Yang, B., Yang, J. and Kitipornchai, S. (2017), "Thermoelastic analysis of functionally graded graphene reinforced rectangular plates based on 3D elasticity", *Meccanica*, **52**(10), 2275-2292. https://doi.org/10.1007/s11012-016-0579-8.

Zhang, Y.W. and She, G.L. (2024), "Nonlinear transient response of rotating graphene platelets reinforced metal foams blades with initial geometric imperfection", *Eng. Struct*., **314**, 118291. https://doi.org/10.1016/j.engstruct.2024.118291.

Zhang, Y.W., She, G.L. and Eltaher, M.A. (2024), "Dynamic characteristics of shape-memory alloy plates immersed in liquid subjected to blast loading", *Ocean Eng.*, **313**(2), 119507. https://doi.org/10.1016/j.oceaneng.2024.119507.

CC